MICRO X-RAY COMPUTED TOMOGRAPHY OF ADHESIVE BONDS IN WOOD

P. E. McKinley*†

Graduate Research Assistant
E-mail: paige.mckinley@oregonstate.edu

D. J. Ching

Graduate Research Assistant
E-mail: daniel.ching@oregonstate.edu

F. A. Kamke*†

Professor and JELD-WEN Chair
Wood-based Composites Science
Oregon State University
Corvallis, OR
E-mail: fred.kamke@oregonstate.edu

M. Zauner

Eidgenössische Technische Hochschule (ETH)
Zürich, Switzerland
E-mail: mzauner@ethz.ch

X. Xiao

Advanced Photon Source
Argonne National Laboratory
Argonne, IL
E-mail: xhxiao@aps.anl.gov

Abstract. Micro X-ray computed tomography (XCT) is an emerging technology that has found many applications in biology and the study of materials. Synchrotron-based micro XCT has been adopted for the study of adhesive bonding in wood. This study reviews recent developments of an integrated project that uses micro XCT to assist with modeling of adhesive bonds and to assess the role of cell wall penetration on moisture resistance. This research includes the study of anatomical features of several commercially important wood species, penetration of three adhesive types into wood, moisture effects on bonding, and mechanical performance of bonds during XCT scanning.

Keywords: Moisture durability, digital volume correlation, digital image correlation, Douglas-fir, X-ray computed tomography.

INTRODUCTION

Penetration of adhesive into the porous structure of wood has long been recognized as an important consideration for developing adhesives, designing bonding systems, and assessing bond performance. For example, assessment of percentage of wood failure is specified in ASTM D905 (2013). Although not the only factor, adhesive penetration will affect the percentage of wood failure. ASTM D905 also provides data for ultimate shear strength but provides no information about shear strain or the location of crack initiation and progression of failure. Unfortunately, a method is lacking for quantitative analysis of

---

* Corresponding author
† SWST member

the effects of adhesive penetration (sometimes referred to as infiltration) on adhesive bond performance, which is the long-term goal of this study. The specific objectives are: 1) develop a numerical model to simulate mechanical behavior of adhesive bonds that quantitatively accounts for the role of adhesive penetration, 2) determine if adhesive penetration into the cell wall has a positive influence on moisture resistance, and 3) create three-dimensional (3D), micron-scale illustrations of wood adhesive bonds and full-field strain for a variety of wood species and adhesive types. To accomplish these objectives, this study integrated micro X-ray computed tomography (XCT) with mathematical modeling to create a close approximation to actual microstructure of an adhesive bond and thus capture the influence of anatomical structure and penetration pattern on mechanical performance of the bond. In addition, this study incorporates in situ mechanical testing during XCT scans, mechanical testing of specimens before and after XCT scans, and moisture cycling of bonded wood specimens for comparison with modeling results. This project is ongoing with a description of the methodology and preliminary results presented here. Details regarding the model development have been previously reported (Nairn et al 2013; Kamke et al 2014).

LITERATURE REVIEW

Studies have shown that the molecular weight (MW) of an adhesive will affect its penetration into wood cell walls (Stephens and Kutscha 1987; Paris and Kamke 2015), and penetration is believed to affect both bond behavior (Frihart 2009; Kamke and Lee 2007) and the deformation of a wood composite under an applied load (Gindl et al 2005). Because of its oligomeric composition, the small molecules of prepolymeric methylene diphenyl diisocyanate (MDI) easily penetrate into the cell wall structure (Frazier 2002). Phenol formaldehyde (PF) is considered one of the most durable adhesives in regard to moisture resistance. The low-molecular weight portion of commercial PF adhesives readily penetrates the cell wall (Stephens and Kutscha

1987). The ability of the phenolic groups to enter the wood cell wall has been proposed to inhibit water infiltration, decrease swelling, and distribute stresses across a broader volume of the bonded assembly (Frihart 2009).

Many light microscopy and scanning electron microscopy (SEM) studies have shown penetration of adhesives into cell lumens, but cell wall penetration is more difficult to detect when present (Kamke and Lee 2007). Nevertheless, penetration of PF into the cell wall has been observed through SEM, ultraviolet microscopy (Gindl 2001), and nanoindentation (Gindl et al 2004). Studies have successfully detected adhesive penetration into the cell wall using techniques such as X-ray fluorescence microscopy (XFM) and nanoindentation (Jakes et al 2015). Preparing thin sections for microscopic observation can destroy the specimen and only reveal a two-dimensional representation. XCT can provide a 3D representation of the adhesive–wood interphase that adequately represents adhesive penetration.

Techniques for micron-scale XCT of biological systems are rapidly advancing. However, few studies have addressed applications with wood. Micro XCT was used to investigate adhesive penetration in laminar wood composites (Modzel et al 2011; Hass et al 2012; Paris et al 2015), medium-density fiberboard (Standfest et al 2010), and particleboard (Evans et al 2010); quantification of penetration of surface coatings into wood (Bessières et al 2013); quantitative determination of moisture-induced strain in earlywood and latewood (Derome et al 2011); measurement of MC and distribution in wood (Li et al 2013); effects of weathering on plywood (Li et al 2015); visualization of wood deformations in three-point bending and calculation of a 3D strain field (Forsberg et al 2010); and observation of compression and tension deformation, including initiation of failure with in situ mechanical testing (Zauner and Niemz 2014).

Digital image correlation (DIC) is an optical measurement used to compute full-field

deformation of a solid surface subjected to applied force. DIC has been successfully used (compared with finite element analysis results) to show differences among the behavior of various adhesives in bonded wood assemblies (Serrano and Enquist 2005) and to assess the strain distribution of bonded wood specimens at a micron scale (Schwarzkopf 2014). Digital volume correlation (DVC) is the 3D extension of DIC. The application of DVC to XCT data obtained for bone tissue was first reported by Bay et al (1999). A study that loaded wood specimens in three-point bending during XCT scanning showed that it was possible to get reasonable full-field strain results without adding an artificial speckle pattern (Forsberg et al 2010). A technique similar to DVC, called affine image registration, was used to investigate moisture swelling of wood during XCT scanning. This technique produced evidence to support the cause of anisotropic swelling (Derome et al 2011).

In summary, previous research has indicated that micro XCT and noninvasive image correlation techniques could be useful to study micromechanical behavior of adhesive bonds under load or subjected to moisture cycling.

MATERIALS AND METHODS

The wood species used in this study were Douglas-fir (*Pseudotsuga menziesii*), loblolly pine (*Pinus taeda*), and hybrid poplar (*Populus deltoides x trichocarpa*). The tangential surface of the sapwood was freshly planed and pressed the same day. More information on the exact procedures can be found in Paris et al (2014). Samples were selected to reveal earlywood and/or latewood at the bonded interface.

We chose three experimental adhesives to provide a broad range of adhesive penetration: PF with low MW (18,110 g/mol; polydispersity index = 1.097), PF with high MW (28,050 g/mol; polydispersity index = 1.135), and MDI (Rubinate M, Huntsman, formulated for oriented strandboard). Because none of these adhesives provide adequate X-ray absorption contrast in the reconstructed XCT images, each

Table 1.   Experimental design for macroweathering specimens, with and without accelerated weathering, all specimens are parallel laminated and previously tested in lap-shear.[a]

Wood species	Bonded surface	Adhesive
Douglas-fir	EW:EW	IPF/high MW
Douglas-fir	EW:LW	IPF/high MW
Douglas-fir	LW:LW	IPF/high MW
Douglas-fir	EW:EW	IPF/low MW
Douglas-fir	EW:LW	IPF/low MW
Douglas-fir	LW:LW	IPF/low MW
Douglas-fir	EW:LW	IpMDI
Douglas-fir	LW:LW	IpMDI
Douglas-fir	EW:LW	IPF/low MW with filler and extender

[a] EW, earlywood; LW, latewood; IPF, iodinated phenol formaldehyde; MW, molecular weight; IpMDI, iodinated polymeric methylene diphenyl diisocyanate.

was chemically tagged with iodine (Paris et al 2014, 2015; Paris and Kamke 2015). As a result, the working properties of these adhesive systems are different from commercial resins. However, the purpose of this study was to develop a mathematical model and to achieve verification of the model with any adhesive system that shows penetration into the cell wall. In all cases, the adhesive was applied at 120 g/m^2 based on resin solids. Bond type and method of evaluation are summarized in Tables 1-3.

Specimens were prepared for two methods of adhesive bond evaluation. The first method focused on the effects of accelerated weathering through two sample types, which are referred to as macroweathering specimens and microweathering specimens.

For the macroweathering specimens, a lap-shear test was adapted from Voluntary Product Standard PS1-09 Structural Plywood (APA 2010), which approximates in-plane shear in tension loading. The specimen dimensions were 6 × 13 × 63 mm (Radial × Tangential × Longitudinal), with bonded length of 13 mm within the lap. This test was performed to failure on dry specimens and specimens of the same type after accelerated weathering. Micro XCT specimens were cut from the failed macroweathering specimens and used for XCT scanning. The micro XCT specimens were approximately 1.8 × 1.8 × 10 mm (R × T × L) and included the

Table 2. Experimental design for microweathering specimens before and after accelerated weathering.[a]

Wood species	Orientation of lamination	Bonded surface	Adhesive
Douglas-fir	Parallel	LW:LW	IPF/high MW
Douglas-fir	Parallel	EW:LW	IPF/high MW
Douglas-fir	Perpendicular	EW:LW	IPF/high MW
Douglas-fir	Parallel	EW:EW	IPF/low MW
Douglas-fir	Parallel	EW:LW	IPF/low MW
Douglas-fir	Parallel	LW:LW	IPF/low MW
Douglas-fir	Perpendicular	EW:LW	IPF/low MW
Douglas-fir	Parallel	EW:LW	IPF/low MW with filler and extender
Douglas-fir	Parallel	EW:LW	IpMDI
Douglas-fir	Parallel	LW:LW	IpMDI

[a] EW, earlywood; LW, latewood; IPF, iodinated phenol formaldehyde; MW, molecular weight; IpMDI, iodinated polymeric methylene diphenyl diisocyanate.

bondline. Table 1 describes the variations for the macroweathering specimens.

The microweathering specimens were subjected to cyclic water-soak and drying but no mechanical testing. The purpose of these microweathering specimens was to examine the effects of water on the ability of the bond to resist stresses associated with swelling and shrinking. In this case, the specimens were first XCT-scanned dry (nominal 12% MC), subjected to five cycles of water-soak and drying, and then scanned again. Table 2 describes the variations for the microweathering specimens.

The second method focused on nonweathered, micro lap-shear specimens that were subjected to in situ stepwise loading during XCT scanning. The micro lap-shear specimens had a cross section of approximately 2×2 mm (R $\times$ T) and a bonded length of approximately 5 mm. The specimens were mounted using a two-part epoxy to threaded grips (stainless steel, M4, male/female, hex standoff) for insertion into the mechanical test device. The specimens were

Table 3. Experimental design for micro lap-shear specimens subjected to in situ mechanical testing.[a]

Wood species	Bonded surface	Adhesive
Douglas-fir	EW:EW	IPF
Douglas-fir	EW:LW	IPF
Douglas-fir	LW:LW	IPF
Pine	EW:LW	IPF
Hybrid poplar		IPF
Douglas-fir	EW:LW	IpMDI

[a] EW, earlywood; LW, latewood; IPF, iodinated phenol formaldehyde; IpMDI, iodinated polymeric methylene diphenyl diisocyanate.

equilibrated to laboratory conditions prior to XCT scanning. Table 3 describes the variations for the micro lap-shear specimens.

Accelerated Weathering

Half of the macroweathering specimens were subjected to a weathering cycle based on a modified ASTM D2559 technique (2012). Specimens were placed in a sealed container, submerged in water (approximately $27°C$) at approximately 20 kPa for 15 hr, and then placed in a convection oven at $75°C$ for 9 hr. After being removed from the oven, each specimen was checked for delamination or cracks, and the cycle was repeated five times. Afterward, specimens were stored at $20°C$ and 65% relative humidity (RH) until they were tested. Specimens were weighed before and after weathering.

All microweathering specimens were subjected to XCT scanning before and after accelerated weathering. The procedure consisted of five cycles of water-soak for 30 min at room temperature at approximately 20 kPa absolute pressure, followed by drying for 30 min in an air stream at $70°C$ and less than 1% RH. The specimens were allowed to equilibrate to laboratory conditions for approximately 12 hr after weathering and before XCT scanning.

Macro Lap-Shear Test

Macroweathering specimens were tested to obtain maximum apparent shear stress following a

modified ASTM D2339 (2011) standard and using a universal testing machine in tension mode (E1000; Instron, Norwood, MA). Crosshead movement rate was 0.40 mm/min. During the test, DIC was used to obtain full-field surface displacement measurements around the bondline. Before testing, a speckle pattern was applied using an air deposition technique (Schwarzkopf et al 2013). A stereo-microscope DIC apparatus (Vic 3D Micro, Correlated Solutions, Columbia, SC) was rigidly attached to the universal testing machine to prevent external movement in the cameras (Fig 1). The field of view was roughly 49 mm^2, and spatial resolution was 3.2^2 μm/pixel. Images were recorded every second until failure. The collected data were processed using Vic-Micro 3D 2012 software with a subset size of 49 and a step size of 11. Strain was calculated using the Lagrangian finite strain tensor approximation. Maximum strain and a visual of the surface strain were recorded.
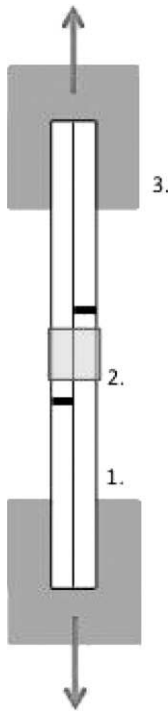

Figure 1.   Lap-shear with digital image correlation (DIC) test setup. (1) Lap-shear test specimen with central bondline (2) Field of view for DIC (3) Instron test grips with direction of loading.

SEM/Energy Dispersive Spectroscopy

An FEI (Hillsboro, OR) Quanta 3D dual beam SEM/focused ion beam was used for SEM and energy dispersive spectroscopy (EDS) analysis to confirm adhesive penetration in lumens and cell walls. Specimens were cut to 2 mm thickness, and the cross-section surface was smoothed with a Leica (Buffalo Grove, IL) UC7 ultramicrotome. The specimens were sputter-coated with gold/palladium, and some had additional osmium coating to prevent charging. A high vacuum was used with a beam energy of 8-10 kV and a spot size of 5. Elemental maps of carbon, oxygen, and iodine were collected to compare only the relative concentration of the adhesive in the sample and to indicate if the iodine was still properly tagged to the adhesive.

Micro XCT

Micro XCT was performed at the beamline 2-BM of the Advanced Photon Source (APS) at Argonne National Laboratory (Argonne, IL). The experiments were performed during two visits, February and October 2014. The microweathering specimens were scanned in February. Additional information about the beamline can be found in Paris (2014). The spatial resolution was determined to be 1.45^3 μm^3/voxel, beam energy 15.5 keV, and exposure time 300 ms. Each scan required approximately 25 min to collect 1500 images, at $0.12°$ increments and a field of view of 2.97^3 mm^3. The scintillator film to specimen distance was 8 mm. Tomograms were reconstructed based on absorption contrast with a fast-filtered back-projection algorithm and stored as image stacks (cross-sectional view) of floating point gray scale slices.

The macroweathering and micro lap-shear specimens were scanned at the APS in October 2014. These specimens were scanned with a resolution of 1.3^3 μm^3/voxel, beam energy 25 keV, and exposure time 150 ms. Each scan took approximately 7 min and collected 1500 images, at $0.12°$ increments and a field of view of $3.33^2 \times 2.77$ mm^3. The scintillator film to specimen

distance was 50 mm. Tomograms were reconstructed using TomoPy (version 0.0.3, Guürsoy et al 2014). Single-distance phase retrieval (Paganin et al 2002) was performed on the phase-contrast projection images before interpolation-based direct Fourier reconstruction (Rivers 2012). The reconstructed slices (cross-sectional views) were stored as floating point gray scale images. Phase-contrast imaging was selected for this experiment in an attempt to improve contrast between cell wall substance and adhesive. In addition, decreasing exposure time decreased scan time and potential specimen motion while under load in the mechanical test device.

In Situ Lap-Shear Test

Micro lap-shear specimens were loaded to failure using a stepwise loading scheme during XCT scanning using a device developed by Zauner and Niemz (2014). The number of scans per specimen varied between three and six because of variability of the bond performance. The intended scan conditions were based on load scenarios: no load, 30% of ultimate load, 60% of ultimate load, plastic deformation, and postfailure. Expected load for each scan was estimated based on preliminary lap-shear testing of similar specimens. During the stepwise loading, the load was applied at a constant rate and closely monitored. When the expected scanning condition was achieved, the device was stopped and the specimen was allowed to rest at a fixed position for 5 min. Then, a full XCT scan was performed before proceeding to the next desired scan position. Because of limitations of the testing device and the variability of the samples, this procedure sometimes led to more or less scans. Specimens were loaded at 0.001 mm/s approaching the first two steps and were slowed to 0.0002 mm/s in anticipation of failure of the specimen. Details regarding the design and operation of the mechanical testing device are reported elsewhere (Zauner and Niemz 2014).

Image Processing and Phase Segmentation

Reconstructed tomographs were converted to 8-bit gray scale image stacks and then segmented by fitting the pixel intensity histogram using a Gaussian mixture model (Farnoosh and Zarpak 2008; Yamazaki 1998 Wikipedia 2015). This capability is widely available through various programs. Matlab was chosen because it also has an extensive image processing library. After fitting a mixture of Gaussians to the histogram (Fig 2b), gray scale values were assigned a phase based on expected order of gray scale
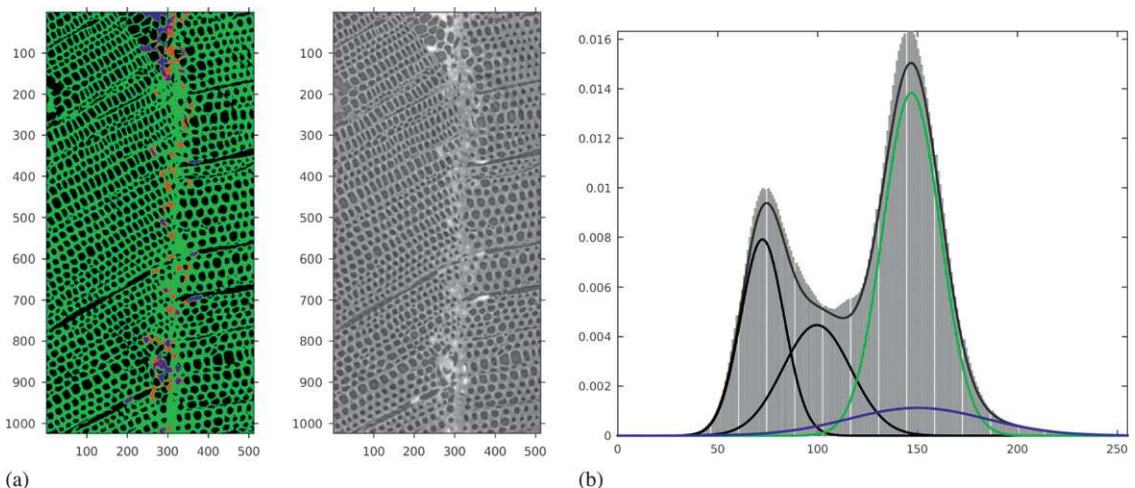

Figure 2. (a) Sample segmented Douglas-fir image. Wood is green, pure adhesive is blue, wood–adhesive mix is red. (b) Histogram of the sample image with four fitted Gaussians overlaid.

(a)   (b)   (c)   (d)
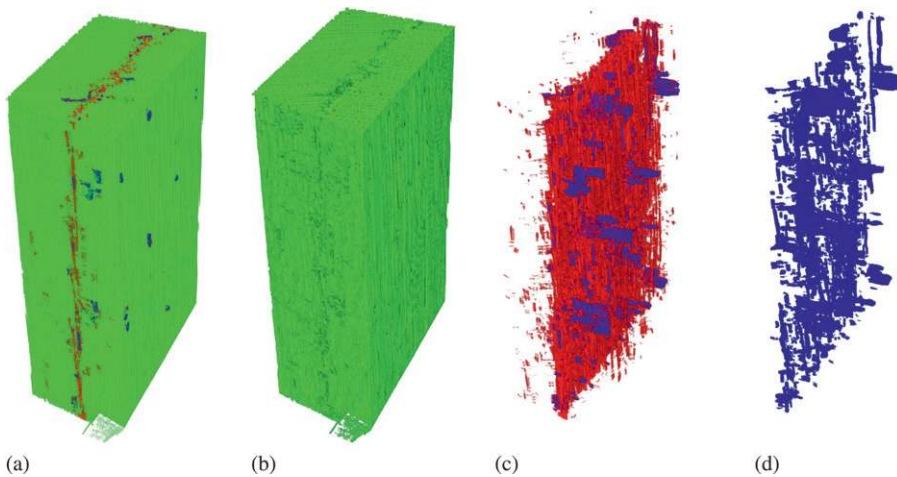
Figure 3.   (a) Three-dimensional section of segmented Douglas-fir. Wood is green, pure adhesive is blue, wood–adhesive mix is red. Low contrast between the background and the wood leads to ring artifacts as seen in the bottom of this section. (b) Only the wood cells. (c) Only pure adhesive and wood–adhesive mix. (d) Only pure adhesive.

intensity. If a phase was assigned a noncontiguous range, the smaller portion of the range was reassigned to its second-most probable phase. Finally, Matlab's 3D island removal algorithm was used to remove unlikely phases, eg adhesive completely surrounded by air. There were five phases to segment given here in order of low to high gray scale value: phase-contrast shadows, air, cell wall, adhesive–cell wall mixture, and pure adhesive. Phase contrast causes dark rings on the outer edge of the cell lumen. These voxels are assigned to the air phase. For hybrid poplar, five Gaussians were identified that matched these phases to the histogram. For pine and Douglas-fir, only four peaks were identified, with the adhesive–cell wall mixture indistinct. The adhesive–cell wall mixture was assigned to a small region on the gray scale range between the cell wall and pure adhesive peaks, at which the probability of a voxel belonging to either was almost equal (Figs 2a and 3).

RESULTS AND DISCUSSION

Macroweathering Specimen Data

Only partial results of the macroweathering specimens are reported here, because the experi-

ment is ongoing. Figure 4 shows an example of the full-field strain measured using the Lagrangian finite strain tensor. All of the images shown here were recorded directly before failure. Observations from these data include a more brittle failure in those with little strain, such as Fig 4c and f although more tests must be conducted before any valid conclusions can be made. The surface strains are of interest because each adhesive should transfer the applied load differently (Serrano and Enquist 2005). We speculated that the adhesives with greater chance of adhesive penetration (low MW iodinated PF (IPF) and iodinated pMDI (IpMDI)) would form an interpenetrating network and reinforce the cell wall. In unpublished work related to Jakes et al (2015), XFM detected brominated PF in the cell wall and significant penetration of iodinated adhesive was also detected in the cell wall. The only way to mechanically observe this phenomenon is to see the deformations across the sample. From this output along with the maximum stress, a comparison will be made for the weathered vs unweathered samples.

SEM and EDS were conducted on all sample types. Examples of the micrographs and elemental maps are represented in Figs 5-7. The elemental maps represent the location of iodine in
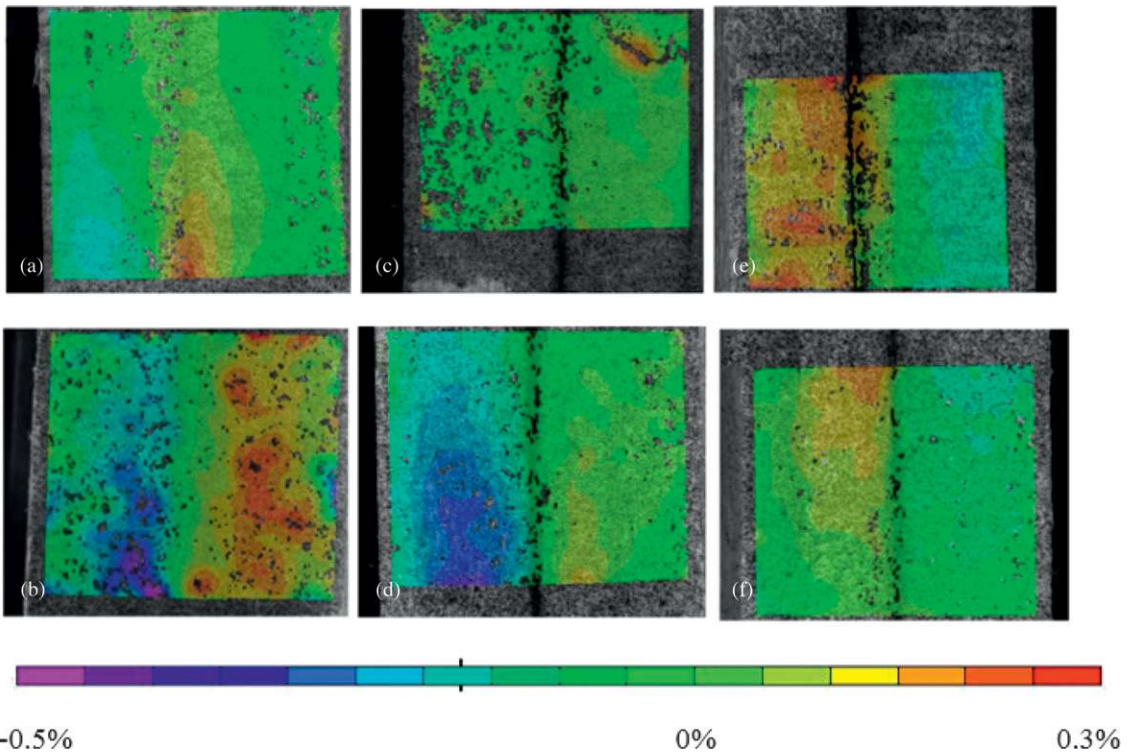
Figure 4. Example digital image correlation surface shear strain maps of Douglas-fir earlywood bonded to latewood specimens with a centrally located bondline and the earlywood laminate located on the left side. (a) iodinated polymeric methylene diphenyl diisocyanate (IpMDI) specimen after accelerated weathering, (b) IpMDI specimen dry, (c) iodinated phenol formaldehyde (IPF) high molecular weight (MW) specimen after accelerated weathering, (d) IPF high MW specimen dry, (e) IPF low MW specimen after accelerated weathering, and (f) IPF low molecular weight specimen dry.
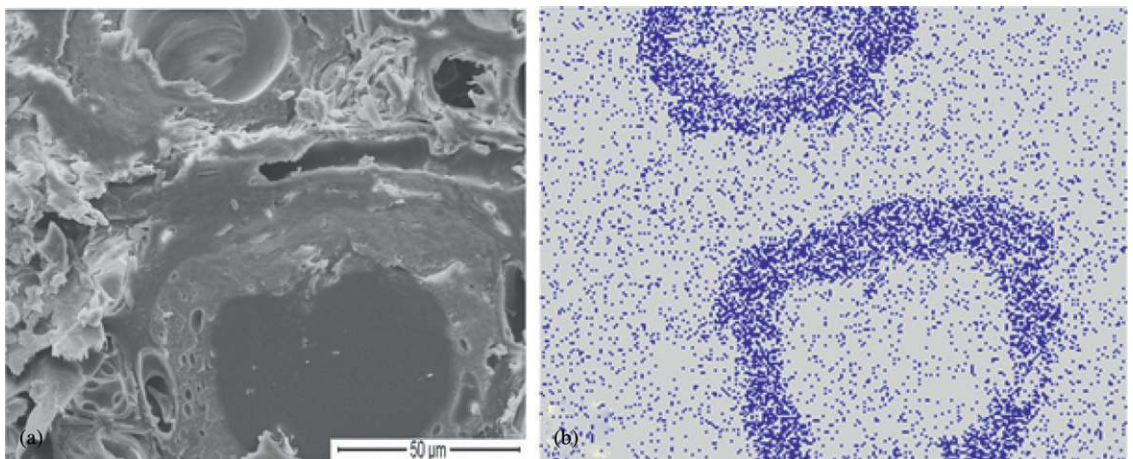
Figure 5. Cross-sectional view of Douglas-fir sample bonded with low molecular weight iodinated phenol formaldehyde, exposed to weathering (this section has a lot of cell wall tear-out but two large lumens lined with adhesive can still be distinguished); (a) scanning electron microscope, scale bar is 50 μm and (b) same view showing elemental map of iodine.
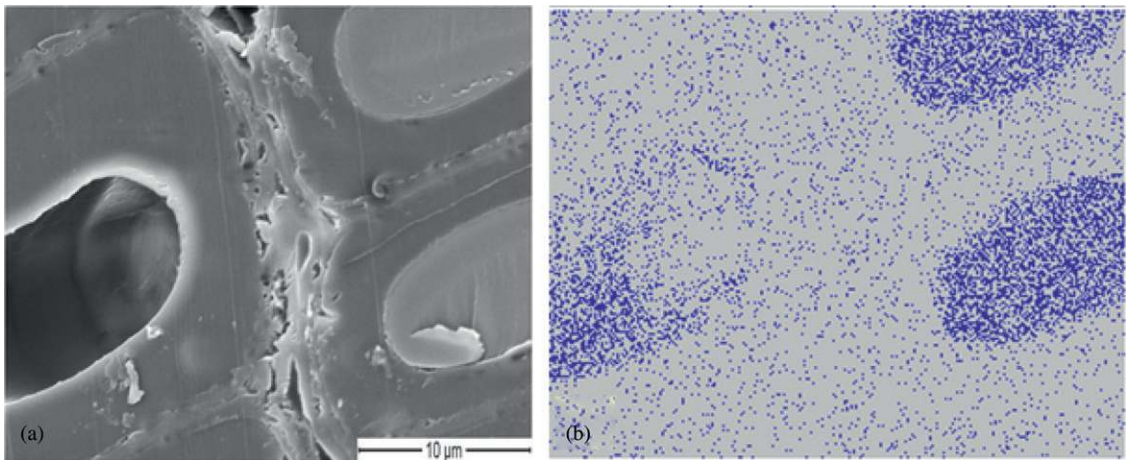
Figure 6.   Cross-sectional view of Douglas-fir specimen bonded with iodinated polymeric methylene diphenyl diisocyanate (IpMDI), exposed to weathering; (a) scanning electron microscope, scale bar is 10 μm and (b) same view showing elemental map of iodine.
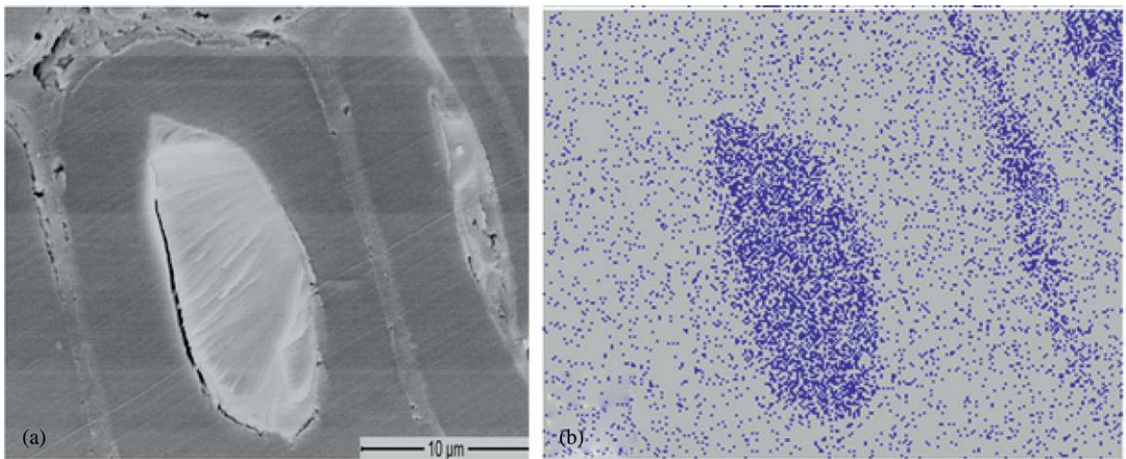

Figure 7.   Cross-sectional view of Douglas-fir specimen bonded with high molecular weight iodinated phenol formaldehyde, never exposed to weathering; (a) scanning electron microscope, scale bar is 10 μm and (b) same view showing elemental map of iodine.

the sample and, therefore, the location of the tagged adhesive. No calibration was performed. Therefore, only the presence but not the concentration of iodine can be confirmed. Because all PF was formulated with iodinated phenol, any PF present will be tagged with iodine. In contrast, only partial tagging of pMDI was achieved. It is possible that some MDI oligomer did not react with the triiodo-phenol. This technique was used to obtain qualitative data and

the location of the iodine in the sample, but no conclusions were made about adhesive penetration into the cell wall.

It was observed that the IpMDI did not provide sufficient X-ray absorption or phase contrast to segment it from the wood cell wall for the macroweathering specimens or the micro lap-shear specimens that were scanned in October 2014 (Fig 8c). However, the same
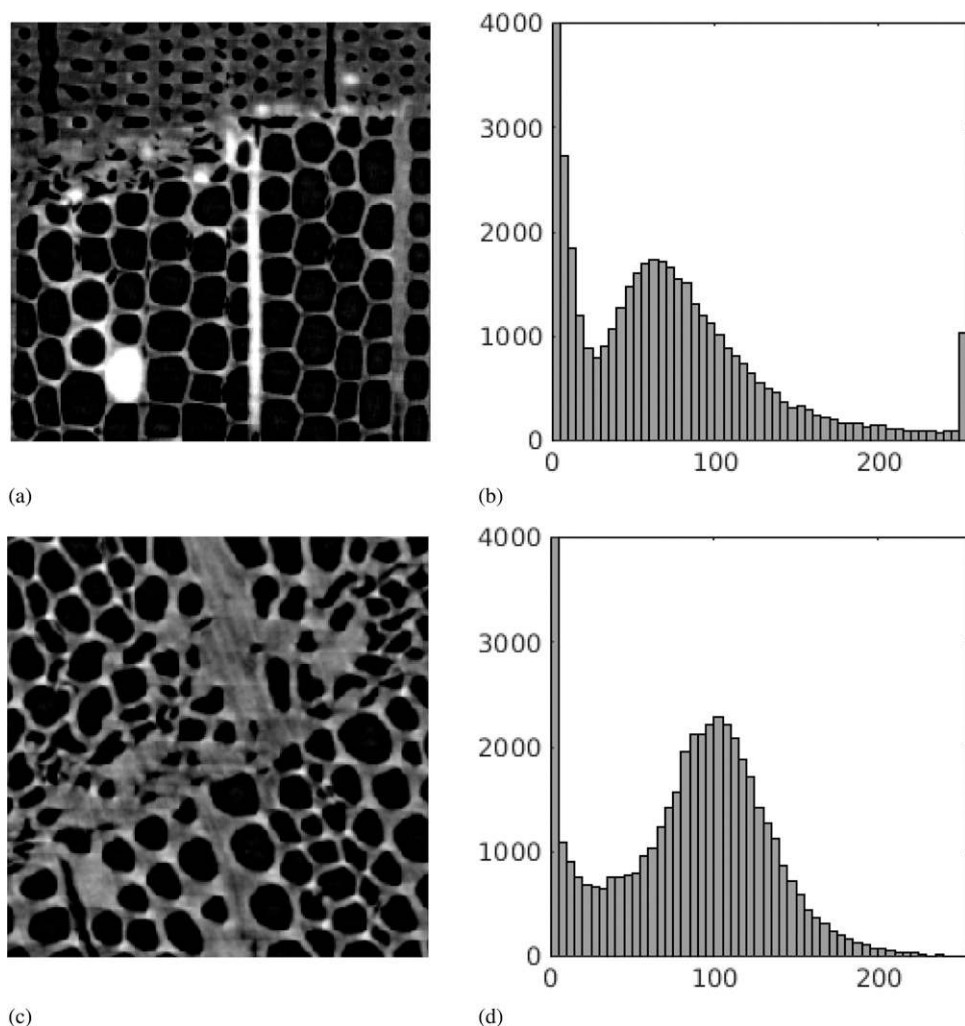
(a)

(b)

(c)

(d)

Figure 8. Comparison of contrast in iodinated polymeric methylene diphenyl diisocyanate (IpMDI) bonded Douglas-fir specimens between February and October 2014. (a-b) Image slice from February and corresponding gray scale histogram. (c-d) Image slice from October and corresponding gray scale histogram (c-d).

adhesive formulation provided excellent X-ray adsorption in the IpMDI microweathering specimens that were scanned in February 2014 (Fig 8a). EDS confirmed the presence of iodine in the October specimens. October scans were performed with higher beam energy, shorter exposure time, and greater scintillator film to specimen distance. We speculated that the higher beam energy resulted in poor contrast between the cell substance and the adhesive, but further investigation is needed. A qualitative comparison of our XCT results that did provide suffi-cient contrast could be made with similar experiments conducted on beech wood (Hass et al 2012).

DVC with Wood

Forsberg et al (2010) were successful in calcu-lating sensible displacement and strain data from a wood specimen in three-point bending, but they noted "anomalous deformation patterns ... that can be traced back to the [microstructure] of the wood." This is because DVC relies on randomly
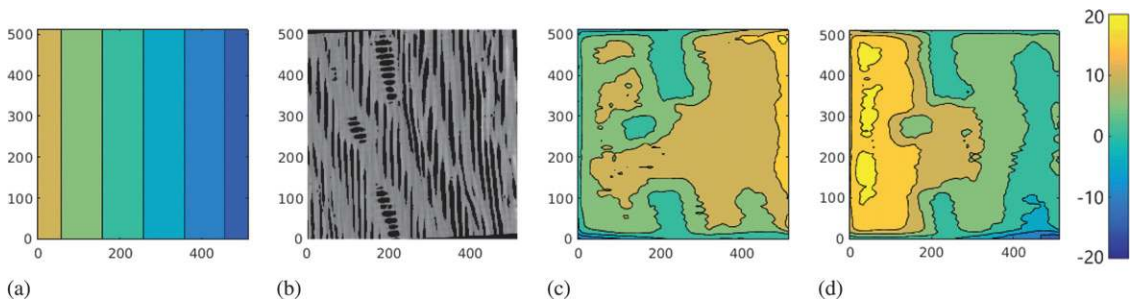
Figure 9.   Artificial simple shear in Douglas-fir latewood along the longitudinal direction with a maximum displacement of ±12 pixels; (a) applied displacement field, (b) slice from the input volume, (c) absolute difference between the applied displacement field and the calculated field from digital volume correlation (DVC), and (d) results of DVC for the slice.

varying intensity gradients for consistent tracking of points through space (Estrada and Franck 2015). On a micron scale, wood has a nearly uniform repeating pattern of characteristic features.

The density of features in a speckle pattern directly relates to the scale on which deformations can be resolved (Bar-Kochba et al 2014). Wood microstructure consists of long empty cells that have a fairly uniform cell wall with the exception of a scattering of bordered pits that were large enough to be resolved with XCT. As a result, there is good intensity variation in the radial and tangential directions but not in the longitudinal direction. As a simple example, Fig 9 shows a slice from a volume artificially deformed in simple shear, with a maximum displacement of 12 pixels along the longitudinal direction. In the regions around the rays, in which the image intensity changes on a scale that is closer to the scale of the deformation, there is better precision than in the other regions, in which the cell lumens are about 100 pixels in length.

Forsberg et al (2010) achieved adequate results from DVC applied to wood micro XCT data because their samples provided sufficient texture density at the scale they were investigating and because of the presence of pits. In this study, the micro lap-shear specimens had most of the displacement in the longitudinal direction and lacked a consistent presence of pits. Because our higher resolution and large adhe-

sive regions make it difficult to consistently find good correlations across the sample, investigation is ongoing to use various methods of processing the tomography data and/or adjusting the DVC parameters. We are currently using the open-source DVC software provided by the Franck Group at Brown University (Providence, RI) (Bar-Kochba et al 2014).

Micro Lap-Shear and Stepwise Loading

The stepwise loading procedure provided the ability to visually track the progression of crack initiation and propagation inside the samples. The images in Fig 10 are corresponding slices of one latewood–latewood Douglas-fir IPF sample as a crack developed in successive scans. The crack initiated in two adjacent tracheids on the left side of the interphase region (left-center Fig 10d). The crack propagated tangentially and longitudinally. The interphase region remained intact.

Weathered and Unweathered Results Comparison

Understanding moisture resistance is achieved through comparing all weathered and unweathered data, including XCT. Figure 11 shows a Douglas-fir, earlywood bonded to latewood sample, cross-laminated with high MW IPF. The crack in the top latewood region propagated after being subjected to five weathering cycles.
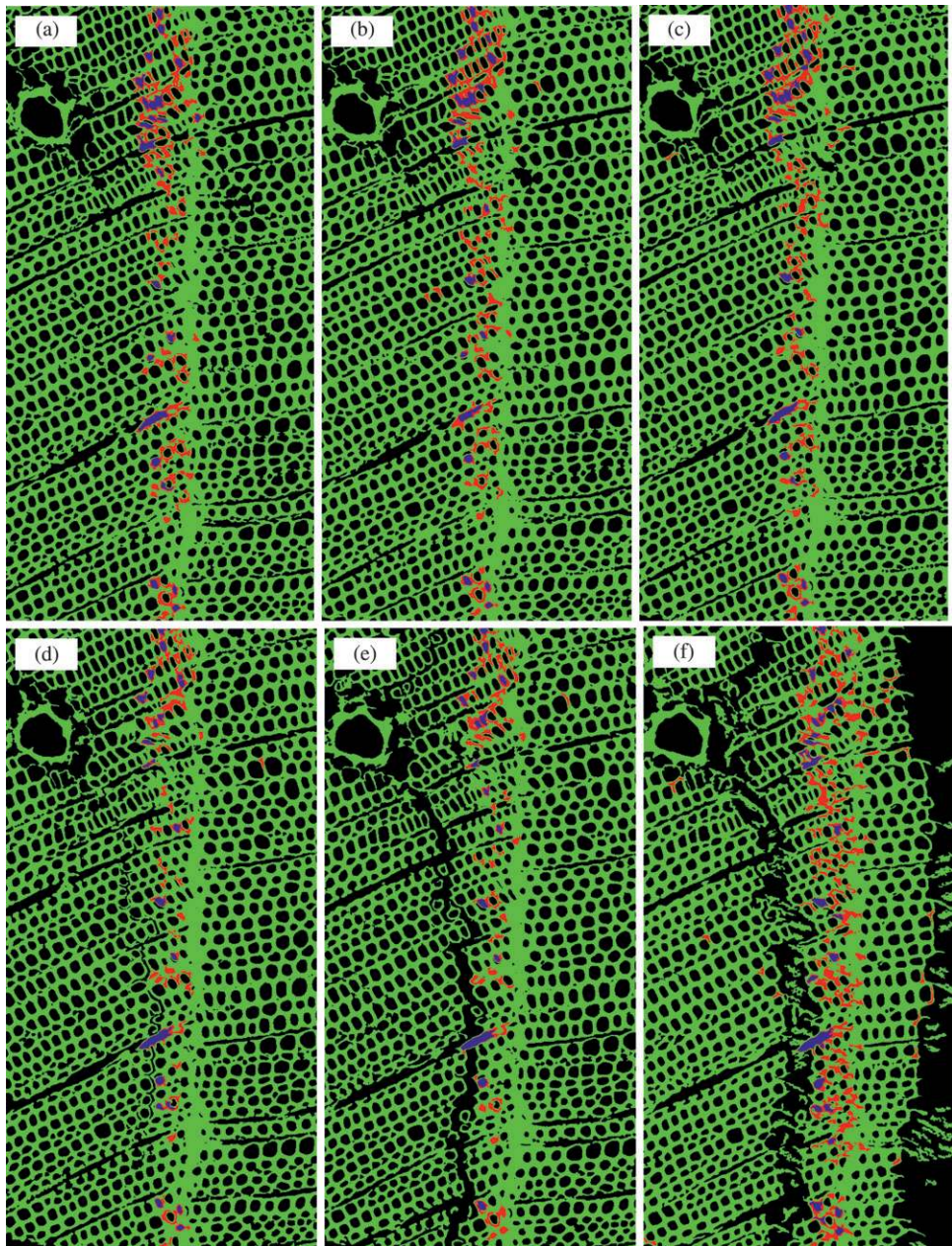
Figure 10. Segmented slice from X-ray computed tomography data of one latewood–latewood Douglas-fir specimen bonded with iodinated phenol formaldehyde; (a) through (f) shows the progression from the unloaded state (a) to crack initiation (d) to failure (f). Wood is green, pure adhesive is blue, wood–adhesive mix is red.

Qualitative information was gathered from the XCT datasets related to crack presence and size for each adhesive before and after accelerated weathering. Micro XCT was also used as a quantitative comparison of adhesive penetration into the cell wall through the previously mentioned segmentation of wood substance, adhesive, and air space (Fig 2).
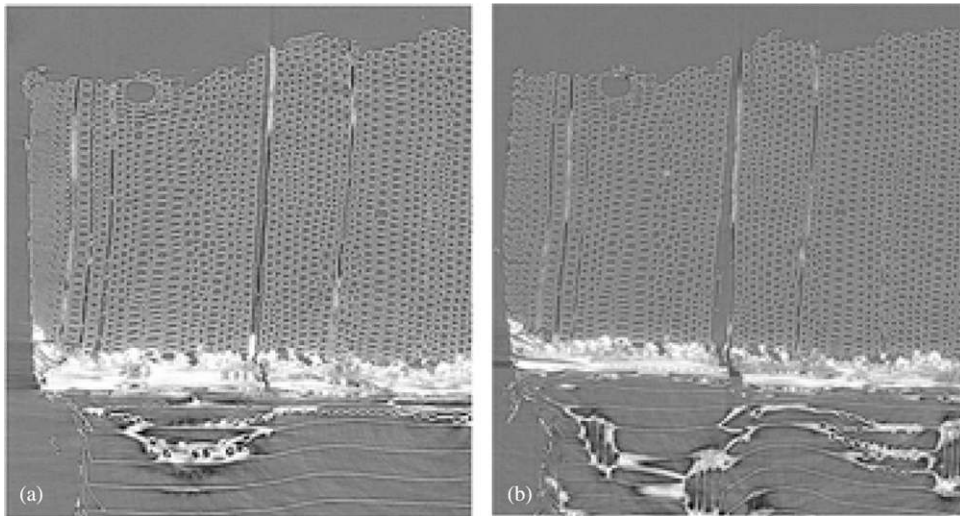
Figure 11.   Slice from reconstructed tomogram of microweathering specimen showing earlywood (bottom) bonded to latewood (top), cross-laminated with high molecular weight iodinated phenol formaldehyde (a) before weathering and (b) after weathering.

The previously scanned micro XCT specimens will be used to prepare nano XCT samples to be scanned on beamline 32-ID at the APS at a resolution of 0.06^3 μm^3/voxel. This information will bring together all investigations from the macro lap-shear performance of the bondline to high-resolution observations of adhesive penetration into the cell wall.

SUMMARY

Techniques have been described that were designed to observe the effects of adhesive penetration on shear performance and accelerated weathering of bonded wood specimens with a spatial resolution approaching 1 micron. These results are part of a larger study to develop a computational model to simulate adhesive bond performance. The model will be used to inform manufacturers of adhesives and bonded wood products regarding formulation decisions and adhesive selection. Micro XCT data were collected for three wood species and three adhesives types. Examples were provided here to illustrate IPF and IpMDI resin penetration into Douglas-fir. Major challenges faced throughout this project have been generating reliable DVC data from tomographic data sets with inconsistent gray scale contrast. The iodine tag on PF resin provided adequate gray scale contrast in absorption-mode XCT. However, results from X-ray attenuation of IpMDI were not adequate or at best inconsistent. The spatial resolution of micro XCT was not able to discern gradients of tagged resin in the cell wall. EDS did confirm that iodine was present in the cell walls in both the IPF and IpMDI specimens. This study is ongoing and will continue to gather results based on the discussed methods. The next steps include gathering cell wall penetration data through a nano XCT experiment with 60-nm spatial resolution, which should improve clarity with regard to the extent of cell wall penetration. Nanoindentation experiments will complement cell wall penetration results and provide information concerning cell wall modifications for use in the mathematical model. Image processing, DVC, and statistical analysis of our results will be the subject of future studies.

REFERENCES

APA (2010) PS 1-09. Voluntary product standard for structural plywood. The Engineered Wood Association, Tacoma, WA.

ASTM (2013) Standard test method for strength properties of adhesive bonds in shear by compressive loading. D 905-08. American Society for Testing and Materials, West Conshohocken, PA.

ASTM (2011) Standard test method for strength properties of adhesives in two-ply wood construction in shear by tension loading. D 2339-98. American Society for Testing and Materials, West Conshohocken, PA.

ASTM (2012) Standard specification for adhesives for bonded structural wood products for use under exterior exposure conditions. D2559-12a. American Society for Testing and Materials, West Conshohocken, PA.

Bar-Kochba E, Toyjanova J, Andrews E, Kim K, Franck C (2014) A fast iterative digital volume correlation algorithm for large deformations. Exp Mech 55(1): 261-274.

Bay BK, Smith TS, Fyhrie DP, Saad M (1999) Digital volume correlation: Three-dimensional strain mapping using X-ray tomography. Exp Mech 39(3):217-226.

Bessières J, Maurin V, George B, Molina S, Masson E, Merlin A (2013) Wood-coating layer studies by X-ray imaging. Wood Sci Technol 47(4):853-867.

Derome D, Griffa M, Koebel M, Carmeliet J (2011) Hysteretic swelling of wood at cellular scale probed by phase-contrast X-ray tomography. J Struct Biol 173(1): 180-190.

Estrada JB, Franck C (2015) Intuitive interface for the quantitative evaluation of speckle patterns for use in digital image and volume correlation techniques. J Appl Mech 82(9):095001.

Evans PD, Morrison O, Senden TJ, Vollmer S, Roberts RJ, Limaye A, Arns CH, Averduck H, Lowe A, Knackstedt MA (2010) Visualization and numerical analysis of adhesive distribution in particleboard using X-ray micro-computed tomography. Int J Adhes 30(8):754-762.

Farnoosh R, Zarpak B (2008) Image segmentation using Gaussian mixture model. IUST Int J Eng Sci 19(1-2):29-32.

Forsberg F, Sjödahl M, Mooser R, Hack E, Wyss P (2010) Full three-dimensional strain measurements on wood exposed to three-point bending: Analysis by use of digital volume correlation applied to synchrotron radiation micro-computed tomography image data. Strain 46(1):47-60.

Frazier CE (2002) The interphase in bio-based composites: What is it, what should it be? Pages 206-212 *in* Proc 6th Pacific Rim Bio-based Composites Symposium, Portland, OR.

Frihart CR (2009) Adhesive groups and how they relate to the durability of bonded wood. J Adhes Sci Technol 23(4):601-617.

Gindl W (2001) SEM and UV-microscopic investigation of glue lines in Parallam® PSL. Holz Roh-Werkst 59: 211-214.

Gindl W, Schöberl T, Jeronimidis G (2004) The interphase in phenol-formaldehyde and polymeric methylene di-phenyl-di-isocyanate glue lines in wood. Int J Adhes 24:279-286.

Gindl W, Sretenovic A, Vincenti A, Müller U (2005) Direct measurement of strain distribution along a wood bond line. Part 2: Effects of adhesive penetration on strain distribution. Holzforschung 59(3):307-310.

Gürsoy D, De Carlo F, Xiao X, Jacobsen C (2014) TomoPy: A framework for the analysis of synchrotron tomographic data. J Synchrotron Radiat 21(5):1188-1193.

Hass P, Wittel FK, Mendoza M, Herrmann HJ, Niemz P (2012) Adhesive penetration in beech wood: Experiments. Wood Sci Technol 46(1-3):243-256.

Jakes J, Hunt C, Yelle D, Lorenz L, Hirth K, Gleber S, Vogt S, Grigsby W, Frihart C (2015) Synchrotron-based X-ray fluorescence microscopy in conjunction with nanoindentation to study molecular-scale interactions of phenol-formaldehyde in wood cell walls. Appl Mater Interfaces 7(12):6584-6589.

Kamke FA, Lee JN (2007) Adhesive penetration in wood–A review. Wood Fiber Sci 39(2):205-220.

Kamke F, Nairn J, Muszynski L, Paris J, Schwarzkopf M, Xiao X (2014) Methodology for micromechanical analysis of wood adhesive bonds using x-ray computed tomography and numerical modeling. Wood Fiber Sci 46(1):15-28.

Li W, Van den Bulke J, De Windt I, Dhaene J, Van Acker J (2015) Moisture behavior and structural changes of plywood during outdoor exposure. Eur J Wood Wood Prod: 1-11.

Li W, Van den Bulke J, De Windt I, Van Loo D, Dierick M, Brabant L, Van Acker J (2013) Combining electrical resistance and 3-D X-ray computed tomography for moisture distribution measurements in wood products exposed in dynamic moisture conditions. Build Environ 67:250-259.

Modzel G, Kamke FA, De Carlo F (2011) Comparative analysis of a wood adhesive bondline. Wood Sci Technol 45(1):147-158.

Nairn J, Kamke F, Muszyński L, Paris J, Schwarzkopf M (2013) Direct 3D numerical simulation of stresses and strains in wood adhesive bond lines based on actual

specimen anatomy from X-ray tomography data. Pages 110-118 *in* Proc Wood Adhesives, October 9-11, 2013, Toronto, ON, Canada.

Paganin D, Mayo S, Gureyev TE, Miller PR, Wilkins SW (2002) Simultaneous phase and amplitude extraction from a single defocused image of a homogeneous object. J Microscopy 206(1):33-40.

Paris JL (2014) Wood-adhesive bondline analyses with micro X-ray computed tomography. http://hdl.handle.net/1957/46442 (14 July 2015).

Paris JL, Kamke FA, Mbachu R, Gibson SK (2014) Phenol formaldehyde adhesives formulated for advanced X-ray imaging in wood-composite bondlines. J Mater Sci 49(2):580-591.

Paris JL, Kamke FA (2015) Quantitative wood-adhesive penetration with X-ray computed tomography. Int J Adhes 61:71-80.

Paris JL, Kamke FA, Xiao X (2015) X-ray computed tomography of wood-adhesive bondlines: Attenuation and phase-contrast effects. Wood Sci Technol 49(6):1185-1208.

Rivers ML (2012) tomoRecon: High-speed tomography reconstruction on workstations using multi-threading. SPIE Optical Engineering+ Applications. International Society for Optics and Photonics. SPIE Proceedings, San Diego, CA, August 12, 2012.

Schwarzkopf M, Muszynski L, Nairn J (2013) Stereomicroscope optical method for the assessment of load transfer patterns across the adhesive bond interphase. Pages 100-109 *in* International Conference on Wood Adhesives, Toronto, Canada, October 9-11, 2013.

Schwarzkopf MJ (2014) Characterization of load transfer in wood-based composites. http://hdl.handle.net/1957/51765 (14 July 2015).

Serrano E, Enquist B (2005) Contact-free measurement and non-linear finite element analyses of strain distribution along wood adhesive bonds. Holzforschung 59(6):641-646.

Standfest G, Kranzer S, Petutschnigg A, Dunky M (2010) Determination of the microstructure of an adhesive-bonded medium density fiberboard (MDF) using 3-D submicrometer computer tomography. J Adhes Sci Technol 24(8-10):1501-1514.

Stephens S, Kutscha N (1987) Effect of resin molecular weight on bonding flakeboard. Wood Fiber Sci 19(4):353-361.

Yamazaki T (1998) Introduction of EM algorithm into color image segmentation. Proc ICIRS 98:368-371.

Zauner M, Niemz P (2014) Uniaxial compression of rotationally symmetric Norway spruce samples: Surface deformation and size effect. Wood Sci Technol 48(5):1019-1031.